CHROMOSPHERIC-CORONAL COUPLING DURING SOLAR FLARES: CURRENT SYSTEMS AND PARTICLE ACCELERATION

R. M. Winglee, M. E. McKean and G. A. Dulk

Department of Astrophysical, Planetary and Atmospheric Sciences
University of Colorado, Boulder, CO 80309-0391

Abstract

Two-dimensional (three velocity) electrostatic particle simulations are used to investigate the particle heating and acceleration associated with the impulsive phase of a solar flare. A cross-field current in the high corona (which is presumably driven by reconnection processes) is used to initiate the flare. Due to the differential motion of the electrons and ions, currents and associated quasi-static electric fields are generated with the primary current and balancing return current being on adjacent field lines. These currents extend from the corona down into the chromosphere. Electrons can be accelerated to energies exceeding 100 keV on short time scales via the quasi-static fields and wave-particle interactions. The spectra of these electrons has a broken power-law distribution which hardens in time. The spatially separate primary and return currents are closed by the cross-field acceleration of the ambient ions into the primary current region. These ions are then accelerated upwards into the corona by the same quasi-static electric field accelerating the electrons downwards. This acceleration can account for the broadened stationary and weak blue shifted component seen in soft X-ray line emissions and enhancements in heavy ion abundances seen in the solar wind in association with solar flares.

1. Introduction

Energetic electrons produced in the impulsive phase of a solar flare are responsible for a wide range of phenomena, including intense radio, soft and hard X-ray emissions. These emissions can provide important information on the dynamics of the coronal and chromospheric plasma during a flare. Observations of the hard X-ray spectra show that impulsive flares can often be categorized by a hardening of the electron spectrum during the rise and peak of the X-ray emissions and a softening of the spectrum during the decay phase (Dennis, 1988 and references therein). The spectrum can also evolve from a single power to a broken power-law (Lin and Schwartz, 1987). Observations of soft X-ray line emissions from heavy ions, such as Ca XIX and Fe XXV, indicate bulk upward motions of plasma with speeds of the order of 100 – 500 km/s and turbulent velocities exceeding 100 km/s (e.g., Antonucci et al., 1985). In addition to this upflow, the relative abundances of certain heavy ions associated with the flare can change, as indicated by in-situ measurements in the solar wind (Reames et al., 1985; Mason, 1987) and by the relative intensities of certain X-ray line emissions (Doschek et al., 1980; Sylwester et al., 1984).

The above inferred particle acceleration can occur via a variety of processes. The spectrum of the energetic electrons is determined by the characteristics of the acceleration mechanism in the primary energy release site and by their interaction with the coronal and chromospheric plasmas. This interaction can, in turn, lead to the generation of intense waves which can produce

further plasma heating, including the generation of high energy tails. The ambient plasma can also experience strong acceleration and heating via both the quasi-static electric fields and induced wave-fields. In addition to these processes, the chromospheric plasma is subject to collisional heating via precipitating energetic electrons.

To date, models for the particle acceleration and heating have concentrated only on limited aspects of the above processes. Recently, collisionless particle simulations have been used by Winglee et al. (1988a,b) and McKean et al. (1989a,b) to model the propagation of energetic electrons and conduction fronts through the corona, self-consistently with the associated return currents and particle heating. Such simulations allow the inclusion of effects arising from both quasi-static electric fields and wave-particle interactions, thereby allowing more detailed modelling.

The purpose of this paper is to extend the above simulations by including (i) an acceleration mechanism or driver which will allows the dynamics of the primary energetic electrons to be determined self-consistently with the dynamics of the ambient plasma and (ii) a collisional plasma at low-altitudes representing the chromospheric plasma. The properties of the currents in the corona are coupled to the properties of chromospheric plasma since the latter component is important in closing the currents and provides a sink for the energy of precipitating energetic electrons. The present study seeks to determine the particle acceleration associated with both quasi-static electric fields and wave-particle interactions under realistic flare conditions in relation to the above observationally inferred properties including

(i) the electron energy spectrum
(ii) the characteristics of the acceleration and heating of the plasma ions, and
(iii) the change in apparent heavy ion abundances.

The outline of the paper is as follows. The simulation model is outlined in section 2. In section 3, the evolution of the electron distribution is described and compared with spectrum inferred from hard X-ray emissions. In section 4, the properties of the induced acceleration and heating of the plasma ions is described and compared with those inferred from the soft X-ray line emissions and observed changes in abundances. A summary of results is given in section 5.

2. Simulation Model

Because of the complexity, variety and nonlinearities of the processes involved, two-dimensional (three velocity) electrostatic particle simulations are utilized. Such simulations allow a self-consistent treatment of the particle dynamics and the associated electric fields, including the acceleration produced by quasi-static electric fields and heating produced by wave-particle interactions. Two-dimensions in the simulations are important since they allow cross-field transport to be evaluated. This cross-field transport is an important factor in the closure of the currents and the ion dynamics (Winglee et al., 1988).

The assumed plasma profile is shown schematically in Figure 1. The corona is represented by a collisionless plasma on the left half of the simulation system. The density is assumed to increase approximately linearly by a factor of four from the left hand edge (representing high altitudes) to the beginning of the transition region which is 3/5 down the simulation system. The transition region and chromosphere are represented by a collisional plasma where the ion collision frequency increases from 0.4 Ω_H at the beginning of the transition region to 8 Ω_H at the lowest altitudes. The density is assumed to increase by a factor of five across the transition region, giving a total

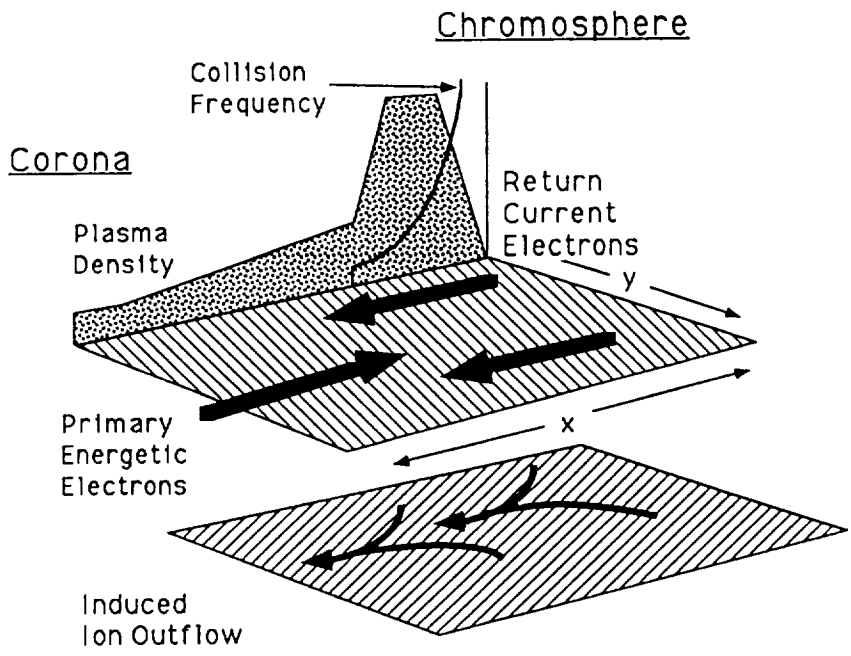

Figure 1. Schematic of the simulation model, including profiles of the density and collision frequency and the induced plasma flows.

increase density of a factor of twenty from the corona to the chromosphere. These changes in density are comparable to those expected in the flaring flux tube and provide a relatively smooth transition from the properties of the coronal plasma to the chromospheric plasma; the exact value of the density increases is not important.

Both plasmas are assumed to be initially in temperature equilibrium with the ion temperature equal to the electron temperature and the coronal temperature equal to 100 eV. The plasma ions are represented by two ion species: H^+ and He^+. The latter represents not only the He but also heavy ion species with charge-to-mass ratios similar to He^+. This heavy ion species is included so that their characteristics in both velocity and coordinate space can be compared with those inferred from observations. For simplicity, variations in the charge-to-mass ratio of an ion due to plasma heating are not considered here. The He ions are assumed to comprise 25% of the plasma. This ratio is higher by about a factor of 2.5 above cosmic abundances although the total charge density associated with the He is comparable to that when the He ions are fully ionized. It is assumed here so that there are sufficient particles for proper statistics for the velocity distribution and density profiles. The following results are not sensitive to the actual relative density provided that it is much less than that of H.

The induced current system and particle acceleration shown in the following are produced by applying a cross-field current at the top of the coronal plasma. Such a current may, for example, arise from reconnection processes in the primary energy release site and is modelled in the simulations by injecting both electrons and energetic ions from the central portion of the left hand boundary. The electrons with their small gyro-radius remain tied to the field lines and carry little perpendicular current. The energetic ions on the other hand have a much larger gyroradius and stream across the field lines to set up the cross-field current.

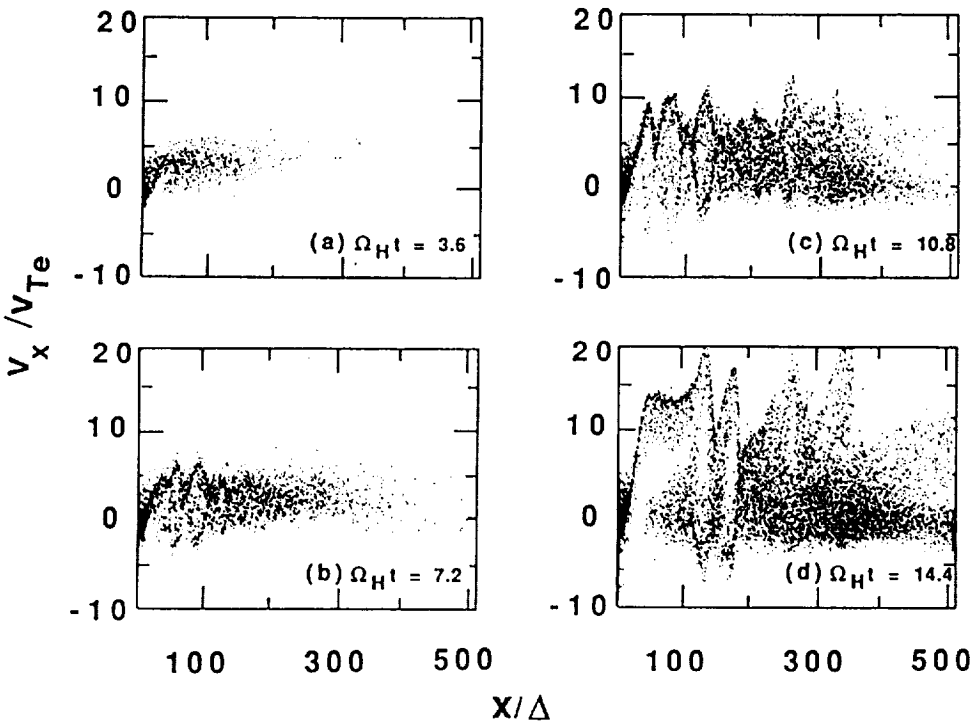

Figure 2. The $v_x - x$ phase space of the beam electrons showing the bulk acceleration and heating when the system is driven by the assumed cross-field current in the corona. Electrons with energies exceeding 40 keV are created on fast time scales.

Thus, in the center of the system (hereafter called the primary current region), there is an excess of electrons while on adjacent field lines (hereafter called the return current region) there is an excess of positive charge (cf. Winglee et al., 1988). This space-charge separation produces fields which accelerate electrons in the primary current regions downwards into the chromosphere and electrons in the return current region up into the corona. It is the formation of this current system and the associated particle acceleration which is addressed in the following.

3. Electron Properties

The downward acceleration of electrons in the primary current region is illustrated in Figure 2 which shows the evolution of the parallel velocity of the beam electrons (i.e., those injected with the energetic ions). The beam electrons which are injected near the left hand boundary with low velocity (i.e., $x/\Delta \simeq 0$ and $\mid v \mid \lesssim 3v_{Te}$) are seen to be accelerated by the quasi-static electric field to bulk velocities of the order of $10v_{Te}$. For a typical coronal temperature of 100 eV, this bulk velocity corresponds to an an energy exceeding 10 keV.

In addition to this bulk acceleration, intense wave are generated as evidence by the vortices in the particle phase spaces in Figure 2. These waves which arise through the beam-plasma interaction accelerates some of the electrons to energies exceeding 40 keV while some of the electrons are slowed

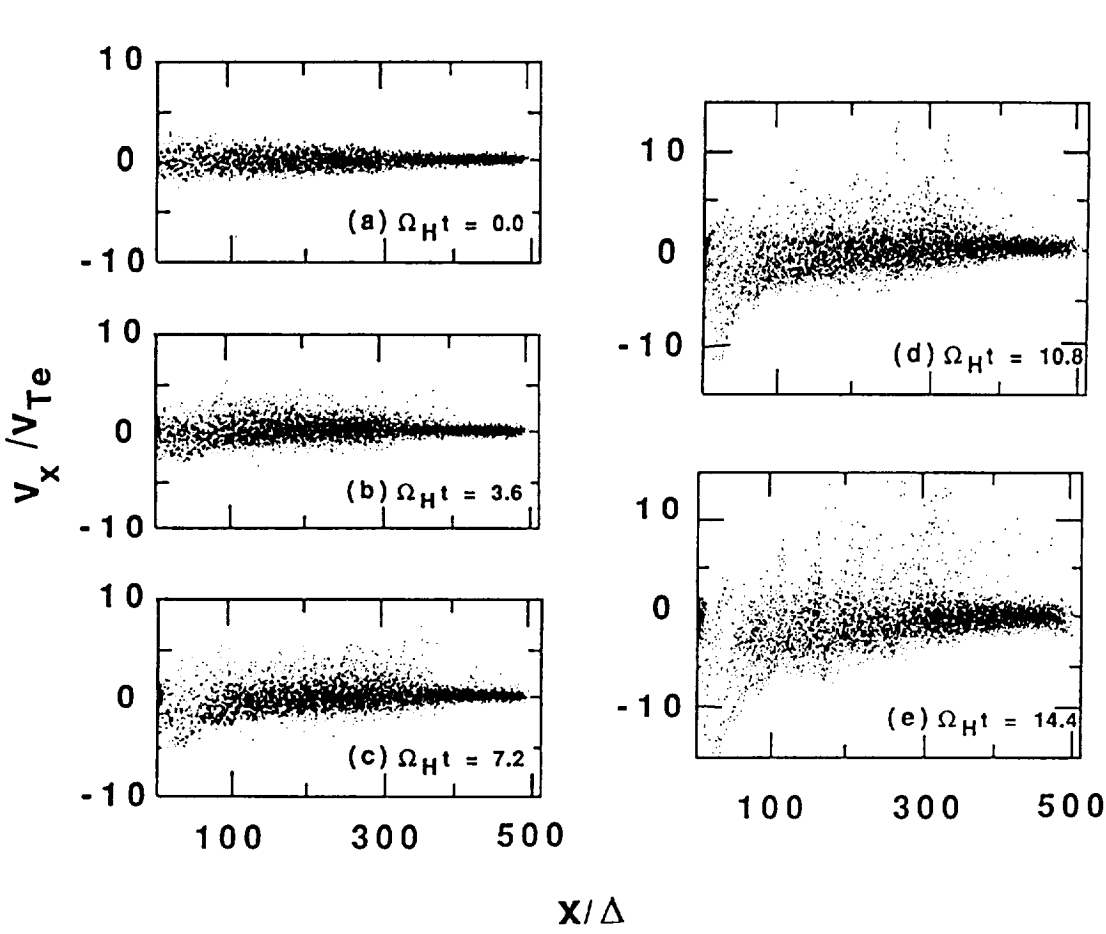

Figure 3. The $v_x - x$ phase space of the ambient plasma electrons. Electrons in the primary current region attain positive velocities of the order of 10 v_{Te} while the return current electrons attain negative velocities of about half the magnitude.

via the interaction, causing the electrons to become dispersed in phase-space, particularly at low altitudes.

The ambient plasma electrons also experience strong bulk acceleration and heating. This is illustrated in Figure 3 which shows the $v_x - x$ phase space of the ambient electrons for the same times as in Figure 2. Electrons in the primary current region are accelerated downwards, attaining positive velocities of the order of 10 v_{Te}, similar to the beam electrons. The return current electrons which are on adjacent field lines are seen in Figure 3 as electrons with negative velocities whose magnitude increases in time. At the end of the simulation their speed is of order of 5 v_{Te} in the corona. This speed is about half the bulk speed of the beam electrons and is sufficient to provide the balancing current since the return current region is twice as large as the primary current region.

Hard X-Ray Characteristics

The predicted spectrum of electrons precipitating into the chromosphere (i.e., $x/\Delta > 200$) is shown in Figure 4. This spectrum is categorized by a broken power law distribution which hardens in time, similar to that observed by Lin and Schwartz (1987). The energy where the break occurs is

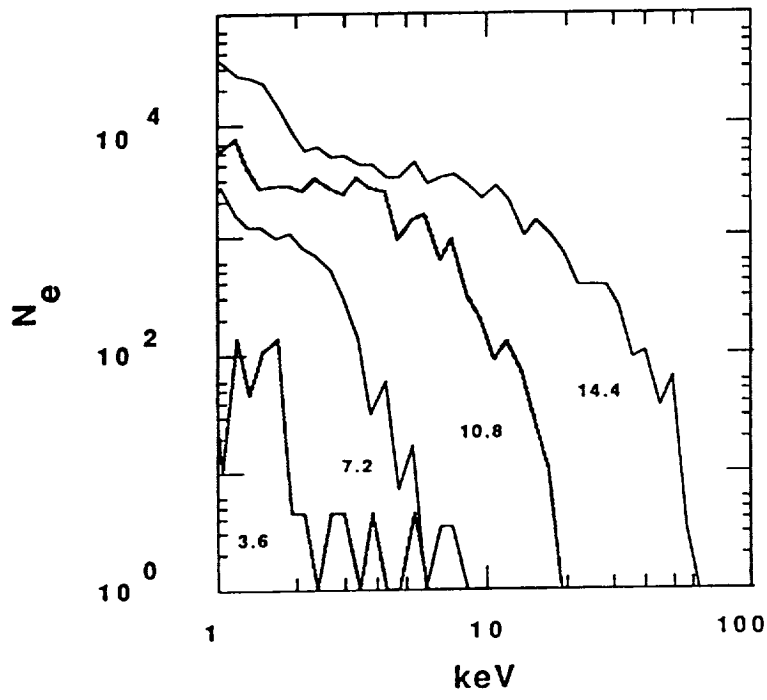

Figure 4. The evolution of the spectrum of electrons impacting on the chromosphere.

indicative of the potential drop associated with the quasi-static electric field in the primary current region.

A unique feature of the present model is that, since the acceleration is driven by quasi-static electric fields extending from the corona down to the chromosphere, the low energy (1 – 10 keV) electrons impact on the chromosphere before the 10 – 100 keV electrons. This prediction differs from acceleration models where the electron acceleration occurs in a limited region in the corona. In this case due to the difference in speeds, the fastest electrons are expected to impact on the chromosphere first.

Another important feature of the model is that the chromosphere is subject to heating before the arrival of the high energy electrons. This heating is seen in Figures 3 c–e as an increase in v_x of electrons at $x/\Delta \gtrsim 400$ and is due to the penetration of the quasi-static fields into the chromosphere on fast time scales. On comparing with Figure 4, the hard X-ray electrons do not arrive until nearly the end of the simulation. The situation is analogous to electrically pulsing a wire: the electric field propagates through at light speed while the actual electrons drift through the wire at much slower speeds. This initial heating of the chromosphere can create electrons exceeding 10 eV and thereby produce $H\alpha$ emissions preceding the rise of the hard X-ray emissions.

4. Ion Properties

The ambient ions are also accelerated by the quasi-static electric fields driving the current system. This acceleration is illustrated in Figure 5 which shows the phase spaces of the H ions as functions across the field in the coronal and transition regions. (The He ions have a similar phase space and are not shown.) In the primary current region, the ions are accelerated upwards reaching peak negative velocities of the order of 10 v_{TH} in the corona (Figure 5b) and about a

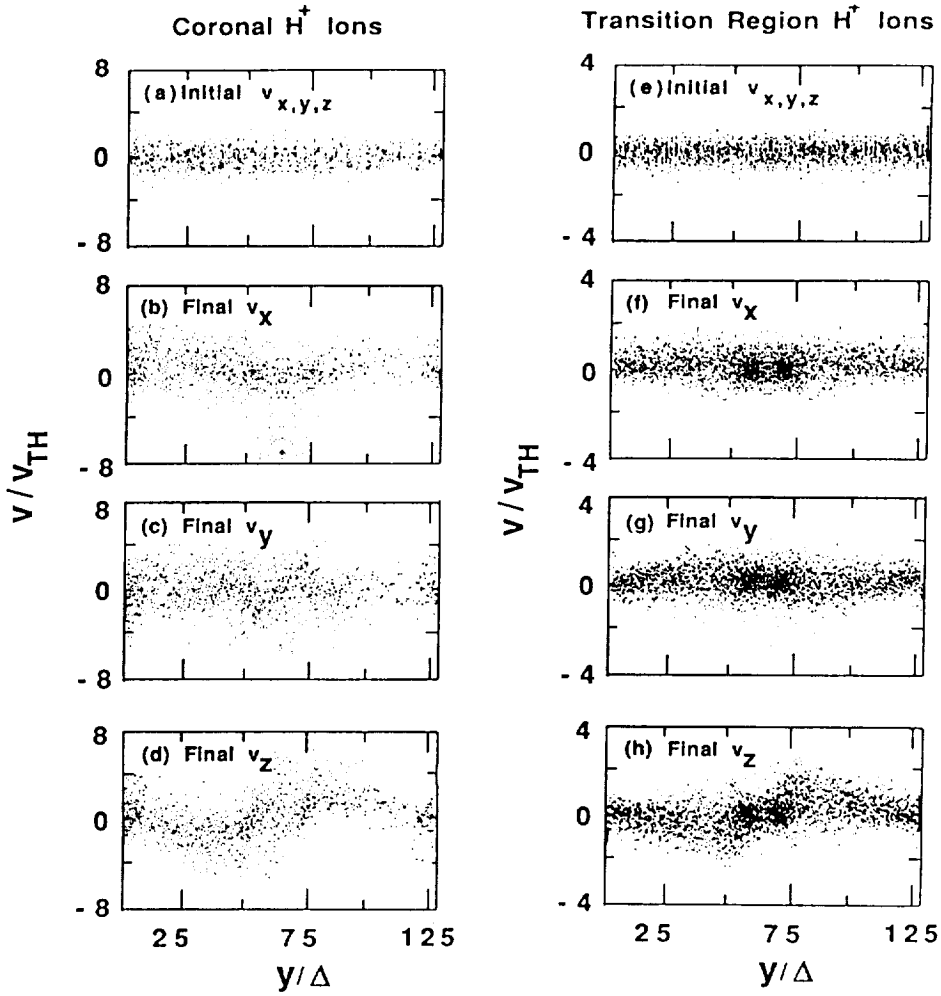

Figure 5. The phase spaces of the H^+ ions in the corona and transition region as functions of position across the field lines, i.e., y, and normalized to the initial thermal speed of the coronal ions v_{TH}.

quarter of this value in the transition region (Figure 5f). In the return current regions, there is some weak acceleration of ions down into the chromosphere.

In addition to this parallel acceleration, the ions experience strong perpendicular acceleration, as seen in the lower panels in Figure 5. This perpendicular acceleration is an integral part of the current system. In particular, since the primary and return currents are not cospatial, a perpendicular current must be drawn in order to close the system. This perpendicular current is most easily carried by the ions which have a larger gyro-radius and hence mobility across the field lines. This current is seen in Figures 5c and 5g as a net flow of ions into the primary current region with ions with $y/\Delta < 64$ having a net positive v_y and ions with $y/\Delta > 64$ having a net negative v_y.

However, even with their larger gyroradius, the ions are still not totally free to propagate across the fields lines and are also subject to strong $\boldsymbol{E} \times \boldsymbol{B}$ drifts in v_z, as seen in Figure 5d and 5h. These drifts can exceed the bulk velocity in y, particularly in the corona. In the chromosphere, the collisions tend to reduce the $\boldsymbol{E} \times \boldsymbol{B}$ drift and enhance the cross-field motion into the primary current region. It is this enhanced cross-field motion which allows the currents to be finally closed.

Soft X-Ray Line Profile Characteristics

The reduced-velocity distributions of the plasma ions convolve with the density of electrons with energies greater than 2 keV are shown in Figure 6. A convolution is taken since the profiles inferred from the soft X-ray line emissions involve a similar convolution. Two viewing angles are shown: a field-aligned viewing angle at 0° and one at 45°. The distributions in each case are integrated over velocities orthogonal to the viewing angle so that for the field-aligned viewing the speed has contributions from the parallel velocity whereas for the cross-field viewing angle which is the most probable, the speed has contributions from both parallel and perpendicular velocity components.

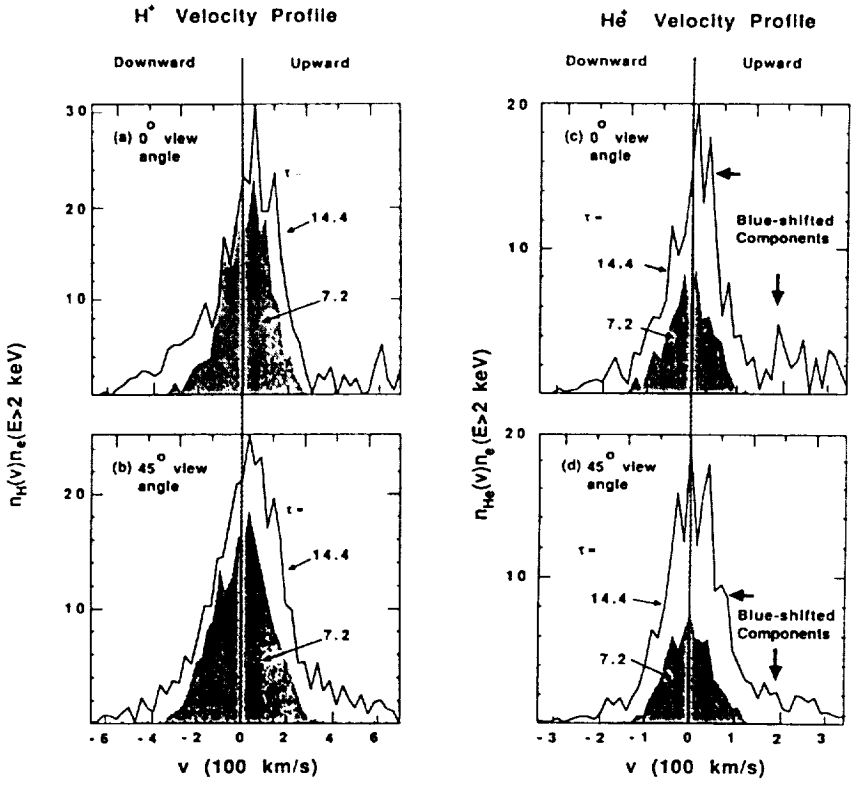

Figure 6. The predicted reduced distributions of the *H* and *He* ions for two different viewing angles.

For both viewing angles, the distribution has a stationary component and a blue-shifted (upward moving component) with the velocity range being comparable to those inferred from observations. Both components are seen to grow in time as the flare evolves, but the stationary component remains the dominant feature, similar to the observations. The stationary component appears broader for the 45° viewing angle due to the perpendicular acceleration and heating of the ions which produces velocity components both in the forward and backward directions, for viewing angles oblique to the magnetic field. As a result of this broadening arising from the perpendicular acceleration and heating, the stationary component appears relatively weak for the cross-field viewing angle.

An additional feature is that the distributions also show the presence of a weak red-shifted component. This component is strongest for the *H* ions and is associated with the downward acceleration of *H* ions in the return current regions. Like the blue-shifted component, this component appears strongest for field-aligned viewing angles.

Changes in Heavy Ion Abundances

Another important characteristic associated with the closing of the current by perpendicular ion acceleration is that changes in the relative abundances of different ion species can result. This change in abundances arises from the fact that the different ion species have different gyroradii, with the heavy ions in low ionization states having the largest gyroradius. Such heavy ions are able to propagate greater across distances from the return current region into the primary current region than the light ions so that a heavy ion concentrations develop in the primary current region and depletions in the return current regions.

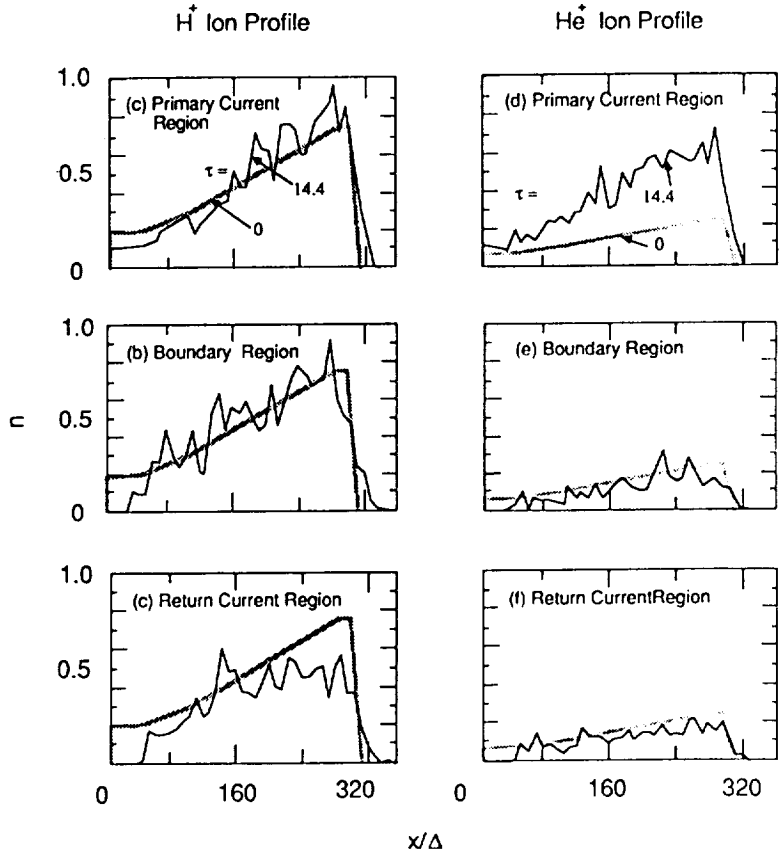

Figure 7. Profiles of the H^+ and He^+ ions at the beginning and end of the simulation at (i) the center of the primary current region, (ii) near the boundary between the primary and return current regions and (iii) in the return current region.

This change in relative abundance is illustrated in Figure 7. The H density in the primary current region changes by only a few tens of percent while the He density is nearly three times larger than its initial density. Since the X-ray emission is dominated by that in the primary current region, the plasma as view from X-ray diagnostics will appear enriched with heavy ions. Moreover, since the outward ion acceleration is dominated by that in the primary current region, the plasma escaping into the solar wind will also appear enriched in heavy ions.

5. Summary

Two dimensional (three velocity) electrostatic particle simulations have been used to investigate the characteristics of the particle acceleration and associated current systems during solar

flares. In the simulations a cross-field current in the high corona (which presumably is driven by reconnective processes) is used to initiate the flare. The results show

(i) the presence of hot electron current channels or primary current regions where the electrons can be accelerated to energies of the order of 100 keV by quasi-static electric fields and wave-particle interactions on short time scales;

(ii) these electrons have a hardening broken power law distribution with the energy at the break indicating the potential associated with the quasi-static electric field;

(iii) return currents are generated on adjacent field lines with the total current matching that of the primary current – this latter requirement implies that the return current electrons are in general less energetic than the beam electrons assuming that the primary current region is narrower than the return current region;

(iv) ions are accelerated across the field lines from the return current regions into the primary current regions to produce current closure - collisions in the chromosphere are particularly important in providing enhanced cross-field transport;

(v) heavy ions in initially low ionization states with their relatively large gyro-radius are preferentially accelerated into the primary current regions which results in enhancements in the abundances of the heavy ions in the X-ray emitting plasma;

(vi) as the ions enter the primary current region they are accelerated upwards by the quasi-static electric field and this field-aligned acceleration results in the blue-shifted component seen in soft X-ray line emissions; broadening of the stationary component is attributed to the perpendicular acceleration of the ions.

Acknowledgements. This work was supported by National Science Foundation grant ATM - 8719371 and by NASA's Solar Terrestrial Theory, Solar Heliospheric and Ionospheric Physics Programs under grants, NAGW-91, NSG-7287 and NAGW-1587 to the University of Colorado. The simulations were performed on the CRAY X-MP at the San Diego Supercomputer Center which is supported by the National Science Foundation.

References

Antonucci, E., Dennis, B. R., Gabriel, A. H., and Simnett, G. M. 1985, *Solar Phys.*, **96**, 129.

Dennis, B. R. 1988, *Solar Phys.*, **118**, 49.

Doschek, G. A., Feldman, U., Kreplin, R. W., and Cohen, L. 1980, *Ap. J.*, **239**, 725.

Lin, R. P., and Schwartz, R. A. 1987, *Ap. J.*, **312**, 462.

Mason, G. M. 1987, *Rev. Geophys.*, **25**, 676.

McKean, M. E., Winglee, R. M., and Dulk, G. A. 1989a, *Proc. Second MAX'91 Workshop*, edited by R. M. Winglee, submitted.

McKean, M. E., Winglee, R. M., and Dulk, G. A. 1989b, *Ap. J.*, submitted.

Reames, D. V., von Rosenvinge, T. T., and Lin, R. P. 1985, *Ap. J.*, **292**, 716.

Sylwester, J., Lemen, J. R., and Mewe, R. 1984, *Nature*, **310**, 665.

Winglee, R. M., Pritchett, P. L., and Dulk, G. A. 1988a, *Ap. J.*, **327**, 968.

Winglee, R. M., Pritchett, P. L., and Dulk, G. A. 1988a, *Ap. J.*, **329**, 440.